Edinburgh Research Explorer

A Tractable Approach to Joint Transmission in Multiuser Visible Light Communication Networks

Link:
Link to publication record in Edinburgh Research Explorer

Document Version:
Peer reviewed version

A Tractable Approach to Joint Transmission in Multiuser Visible Light Communication Networks

Liang Yin and Harald Haas, *Fellow, IEEE*

Abstract—In this paper, an analytical model for the coverage analysis of multiuser visible light communication (VLC) networks is presented, taking into account the cooperation among access points (APs). Specifically, the cooperation is realized through joint transmission (JT), where the coordinated APs jointly transmit data to users in a noncoherent or coherent manner to reduce the inter-cell interference and enhance the useful signal power. Using a second-order moment matching approach, we find approximate distribution functions of the signal power and interference, and derive tractable results for the network coverage probability based on the signal-to-interference-plus-noise ratio (SINR). For both noncoherent and coherent JT, the derived coverage probabiklity are further simplified into closed forms when the communication link is interference-limited. We validate the derived results through Monte Carlo simulations and apply them to study behaviors and trends of the network under various parameter settings. Results show that JT can improve the coverage performance of the network and coherent JT can provide higher performance gains than its noncoherent counterpart, at the cost of higher implementation complexities.

Index Terms—Visible light communication, light-emitting diode, joint transmission, coverage probability, Poisson point process, stochastic geometry.

✦

1 INTRODUCTION

Cisco recently reported that the global mobile data traffic has increased by 63% in 2016, reaching 7.2 exabytes per month [1]. It also forecasts that the global mobile data traffic will experience a sevenfold increase during the next five years [1]. Motivated by this, many industry partners as well as research communities are seeking new technologies that are capable of handling such increasing demand for wireless data traffic. In parallel to many other technologies, visible light communication (VLC) [2], [3], [4], which typically uses intensity modulation and direct detection (IM/DD), has recently emerged and been acknowledged as a promising candidate for future short-range wireless communications. VLC has advantages in implementation cost, operation safety, usable bandwidth, data rate, frequency reuse factor and data security. Extensive studies on point-to-point VLC transmission and reception techniques during the past decade have also led to its recent standardization[1] by the IEEE Computer Society [5].

The femtocell-like deployment of VLC in an indoor environment brings the concept of optical attocells [6], which can be added as an additional network layer, along with the existing radio frequency (RF) counterparts, to future heterogeneous wireless networks. The optical attocell network is a multiuser VLC network, in which each light-emitting diode (LED), or a cluster of LEDs, functions as an access point (AP) to provide wireless data transfer to multiple users within the coverage area. Similar to RF networks, VLC networks are also subject to inter-cell interference, which appears as

- *The authors are with School of Engineering, Institute for Digital Communications, Li-Fi Research and Development Centre, The University of Edinburgh, Edinburgh, EH9 3JL, U.K.*
  Email: l.yin@ed.ac.uk and h.haas@ed.ac.uk.

1. This standardization is currently being revised.

a key limiting factor of the network performance. Based on the fact that signals transmitted through radio waves and through visible light exhibit different propagation characteristics, existing results obtained for RF networks can not be directly applied to VLC networks.

1.1 Related Work and Motivation

On the one hand, by modeling the location of LEDs with the regular grid pattern, the performance of VLC networks is usually evaluated with the aid of computer simulations due to the analytical intractability of the grid model [6], [7], [8], [9], [10]. On the other hand, based on the observation that modern LED lights are commonly installed with built-in motion sensors to reduce the energy consumption, LED lights that detect no occupancy within the coverage area are therefore automatically switched off. Also, even when all LED lights in the network are switched on, the LEDs that are not requested for wireless data transfer do not contribute as the source of interference. Therefore, in most practical scenarios, a thinning process needs to be applied to the locations of LEDs for modeling VLC APs. Such a thinning process is stochastic because it depends on the user locations as well as their mobility profile, both of which are random in nature. Accurate modeling of VLC APs using the described approach remains an open research topic. To facilitate the derivation of tractable results and obtain system design insights, stochastic models [11], [12], [13], [14] have been widely adapted as a suitable method, in which the variable density of active users is effectively captured by the density active transmitters. Specifically, the Poisson point process (PPP) is utilized in this work as it has been shown to yield similar results to the traditional grid model [15] while being more analytically tractable.

With the use of PPP models, the performance of multiuser VLC networks has recently been studied in [15], [16].

The distribution function of the signal-to-interference-plus-noise ratio (SINR) studied in [15] was given as a sum of Gamma densities, whose calculation requires Gram-Charlier series expansion and Laguerre polynomials. As a result, the computation would involve complicated integrals and an infinite number of sums. In [16], the coverage probability of a typical user inside the VLC network was derived using the statistical-equivalent transformation, and the result was given in a tractable form.

Coordinating multiple APs in the network, a technique commonly known as the coordinated multipoint (CoMP) [17], is capable of improving the performance of the network. The coordination and data exchange among APs are supported by an additional backbone network, which can be realized using a wired Ethernet or existing power lines, i.e., via power line communication (PLC) [18], [19]. By making use of the shared information among cooperative APs, inter-cell interference can be effectively mitigated or even converted into useful signals. Since the cooperative APs can be viewed as a virtual multiple-input multiple-output (MIMO) system, CoMP is also named cooperative MIMO, which allows limited bandwidth to be more efficiently utilized among multiple users.

The exact form of CoMP varies from coordinated scheduling/beamforming (CS/CB) to joint transmission (JT), depending on the specific architecture and deployment of the network. In JT, APs can communicate and exchange information, which includes control signals as well as user data and channel state information (CSI), among each other through the backhaul link. This results in an alleviation of the interference level and an enhancement of the useful signal power. Therefore, the implementation of JT in VLC networks can significantly improve the roaming experience of cell-edge users. The realization of JT can generally be classified into two categories: coherent JT and noncoherent JT. In coherent JT, it is assumed that cooperated APs share detailed CSI to the user of interest. Based on the shared CSI, signals are jointly precoded, i.e., using zero-forcing (ZF) precoding, with prior phase alignment and synchronization so that the received signals are coherently constructed in amplitude [17], [20], [21]. In noncoherent JT, signals are transmitted from multiple APs without phase-mismatch correction or synchronization. Instead, soft-combining techniques are utilized for signal detection, yielding an increment in the useful signal power [17], [20], [21].

The performance of noncoherent JT and coherent JT in RF cellular networks has been analytically studied in [22] and [23], respectively. In both works, base stations (BSs) are assumed to be independently distributed according to the PPP, and the coverage probability has been derived. Since the vertical distance of the communication link in RF networks is typically much smaller than the horizontal distance, a planar network model is generally used [22], [23]. However, in typical VLC networks, the size of optical attocells is in the oder of meters. This indicates that a three-dimensional (3D) network model taking into account both the horizontal and vertical distances of the communication link is necessary. For this reason, the coverage analysis of 3D VLC networks is more challenging than that of two-dimensional (2D) RF networks.

1.2 Contributions

The contributions of this paper are as follows.

1) We present a 3D attocell model for the coverage analysis of multiuser VLC networks, taking into account the cooperation among APs. By studying the approximate distribution functions of the signal power and interference through second-order moment matching, analytical expressions for the coverage probability with noncoherent/coherent JT are derived in generally tractable forms and also validated through computer simulations.

2) We show that for typical receiver noise levels, the SINR can be approximated by the signal-to-interference ratio (SIR), based on which expressions for the coverage probability with noncoherent/coherent JT are further simplified into closed forms.

3) We investigate the impact of various key parameters on the network performance and study the achievable performance gain of coherent JT over noncoherent JT under different parameter settings. These findings are useful for studying behaviors and trends of the network and providing guidelines for the design of practical VLC networks.

1.3 Paper Organization

The remainder of this paper is organized as follows. Section 2 describes the presented 3D attocell model and formulates the SINR expression for noncoherent/coherent JT. In Section 3, the approximate distributions of the signal power and interference are investigated and utilized for the coverage probability analysis. Simulation results, together with discussions on the impact of various key parameters on the coverage performance of the network, are presented in Section 4. Finally, concluding remarks are given in Section 5.

2 SYSTEM MODEL

We consider the downlink transmission of a multiuser VLC network, with full frequency reuse, over a confined 3D indoor space. As depicted in Fig. 1, APs are attached to the room ceiling and their horizontal locations are modeled by a 2D homogeneous PPP $\Phi_a = \{x_i, i \in \mathbb{N}^+\} \subset \mathbb{R}^2$, with node density λ_a, where x_i is the horizontal distance between AP i and the origin[2]. The 3D coordinate of a mobile user is constructed by a 2D coordinate plus a vertical variable L, which represents its vertical separation from the ceiling. The variable L can be tuned to model a user at different heights. If, on the other hand, the vertical parameter follows a certain distribution, the presented analysis still applies but the final result should be obtained with an additional integration with respect to L. Based on the user-centric AP cooperation [9], users are assumed to be served by a cluster of APs that are within the cooperation region. We define the cooperation region as a 2D ball centered around the user with radius D. For example, for the user located at the origin

---

2. We define the room center as the origin and use both notions interchangeably throughout the paper.

TABLE 1
Summary of Notation

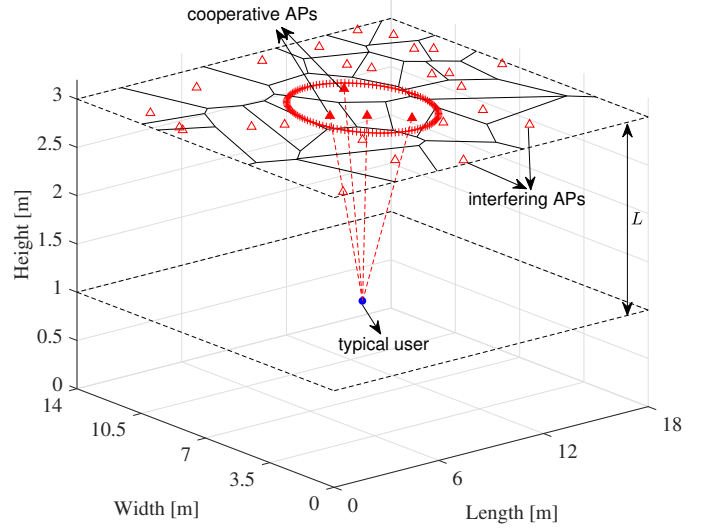| Notation	Description (default value [2], [24], [25])
A_{pd}	effective detection area of the PD (1 cm^2)
b and $\bar{b}$	a 2D ball and its complement
d	Euclidean distance
D	cooperation radius
f_X, F_X and $\mathcal{F}_X$	the PDF, CDF and the characteristic function of variable X
G_c	optical concentrator gain
G_f	optical filter gain (1)
I	normalized interference power
L	vertical distance from the typical user to the ceiling (2 m)
m	LED Lambertian order
n_c	reflective index of the optical concentrator (1.5)
P_{tx}	transmit signal power (1 W)
S	normalized signal power
T	SINR target
x_i	horizontal distance from AP i to the origin
η	responsivity of the PD (0.4 A/W)
μ	the standard Lebesgue measure
λ_a	density of APs
Φ_a	the PPP for APs
Ψ_{fov}	FOV of the PD (90°)
$\Psi_{1/2}$	LED semi-angle (60°)
σ_n^2 and $\bar{\sigma}_n^2$	noise variance (−117.0 dBm) and normalized noise variance
θ_{tx} and θ_{rx}	angle of irradiance and angle of incidence
k_X and θ_X	the shape and scale parameters of a gamma distributed variable X
a_X, d_X and θ_X	the shape and scale parameters of a generalized gamma distributed variable X

Fig. 1. Illustration of the 3D network model with Voronoi cells. APs that are inside the ball $b(o, D)$ jointly transmit data to the typical user. APs that are outside ball $b(o, D)$ act as the source of interference. For simplicity, only the typical user in the centering Voronoi cell is shown. Other users are connected to their nearest APs in a similar manner.

o, the cooperation region can be written as $b(o, D)$. Similarly, the region outside the cooperation ball is denoted by $\bar{b}(o, D)$. Note that in this model, D serves as a tunable parameter to control the number of cooperative APs, which reflects the limited backhaul capacity of practical VLC networks. We focus on the analysis of a *typical* user located at the origin because according to Slivnyak's theorem [11], this typical user can reflect the average performance of users in the network. Note that we do not explicitly consider room boundaries as their impact on network-cell users can be taken into consideration by adjusting λ_a appropriately [16]. Due to the homogeneity of Φ_a, the number of cooperative APs inside ball $b(o, D)$ still follows a Poisson distribution, whose probability mass function (PMF) is:

$$\mathbb{P}\left[\sum_{x_i \in \Phi_a} \mathbf{1}_{b(o,D)}(x_i) = n\right] = \frac{(\pi \lambda_a D^2)^n}{n!} \exp\left(-\pi \lambda_a D^2\right), \quad (1)$$

where $\mathbf{1}_{b(o,D)}(x_i)$ is the random counting measure of ball $b(o, D)$, defined as:

$$\mathbf{1}_{b(o,D)}(x_i) = \begin{cases} 1, & x_i \in b(o, D) \\ 0, & \text{otherwise} \end{cases}. \quad (2)$$

In VLC, the communication channel between an AP and a user consists of the line-of-sight (LOS) link and non-line-of-sight (NLOS) links, that are caused by light reflections of interior surfaces in the indoor environment. However, in a typical indoor environment, the signal power of NLOS components is significantly lower than that of the LOS link [2], [3], [25]. As a result, for a VLC system using tens of MHz modulation bandwidth, the channel frequency

response can be approximated as flat. Since the incisive modeling of link blockage in VLC networks still remains an open research topic, it is not considered in this work. Without loss of generality, the VLC AP is assumed to follow the Lambertian radiation profile, whose transmit power is P_{tx} and Lambertian order is $m = -1/\log_2(\cos(\Psi_{1/2}))$, where $\Psi_{1/2}$ denotes the semi-angle of the LED. The photodiode (PD) equipped at each user is assumed to be facing vertically upwards with a field-of-view (FOV) of Ψ_{fov}. Note that with this assumption, APs that are close to a given user typically result in a high received signal strength (RSS). Since the modeling of receiver orientations is still an open research topic, characterizing the performance of VLC networks with arbitrarily oriented PDs will be the subject of future work. For the LOS link, the direct current (DC) gain of the VLC channel is given by [24]:

$$h = \frac{(m+1)A_{pd}\eta}{2\pi d^2} \cos^m(\theta_{tx})G_f(\theta_{rx})G_c(\theta_{rx})\cos(\theta_{rx}), \quad (3)$$

where d is the Euclidean distance between the transmitter and receiver; A_{pd} denotes the effective detection area of the PD; η is the responsivity of the PD; θ_{tx} and θ_{rx} are the angle of irradiance and the angle of incidence of the link, respectively; $G_f(\theta_{rx})$ represents the gain of the optical filter used at the receiver front end; and $G_c(\theta_{rx})$ represents the gain of the optical concentrator, whose value can be calculated from [24]:

$$G_c(\theta_{rx}) = \begin{cases} \frac{n_c^2}{\sin^2(\Psi_{fov})}, & 0 \leq \theta_{rx} \leq \Psi_{fov} \\ 0, & \theta_{rx} > \Psi_{fov} \end{cases}, \quad (4)$$

where n_c is the reflective index of the optical concentrator, and it is defined as the ratio of the speed of light in vacuum and the phase velocity of light in the optical material. For visible light, typical values for n_c are between 1 and 2.

Based on the geometric property of the VLC link, the channel gain from AP i to the typical user can be simplified to [26]:

$$h_i(x_i) = \alpha \left(x_i^2 + L^2 \right)^{-\frac{m+3}{2}}, \qquad (5)$$

where $\alpha = (m+1)A_{\mathrm{pd}}\eta G_{\mathrm{f}}(\theta_{\mathrm{rx},i})G_{\mathrm{c}}(\theta_{\mathrm{rx},i})L^{m+1}/2\pi$. The VLC receiver is subject to noise processes that include both shot noise and thermal noise. Overall, they can be modeled as the additive white Gaussian noise (AWGN) with power σ_{n}^2 [2]. It is assumed in the system model that the backhaul link can provide error-free coordination and data exchange. However, a backhaul link in practical applications may have delivery latency and limited capacity. The latency affects the duration for which the CSI remains valid, depending on user mobilities. In fact, apart from the feedback scheduling delay, additional backhaul latency can be caused by hardware limitations and the necessary time required for signal processing. The second limiting factor is the backhaul capacity, which should be much larger than the downlink delivery rate because not only the CSI but also the user data need to be shared among cooperative APs.

2.1 Noncoherent Joint Transmission

In the case of noncoherent JT, a user receives multiple copies of the same signal transmitted by a cluster of cooperative APs. In this scheme, accurate synchronizations and CSI are not required at the cooperative APs. Therefore, noncoherent JT has lower implementation complexity and requires less backhaul capacity when compared to its coherent counterpart. At the receiver side, the received copies of signals are combined by accumulating their powers [21], [22]. The achieved SINR at the typical user under the noncoherent JT scheme can be formulated as:

$$\mathrm{SINR} = \frac{\sum\limits_{x_i \in \Phi_{\mathrm{a}} \cap b(\mathrm{o}, D)} \left(x_i^2 + L^2 \right)^{-(m+3)}}{\sum\limits_{x_i \in \Phi_{\mathrm{a}} \cap \bar{b}(\mathrm{o}, D)} \left(x_i^2 + L^2 \right)^{-(m+3)} + \bar{\sigma}_{\mathrm{n}}^2}, \qquad (6)$$

where $\bar{\sigma}_{\mathrm{n}}^2 = \sigma_{\mathrm{n}}^2/P_{\mathrm{tx}}\alpha^2$ is defined as the normalized noise power.

2.2 Coherent Joint Transmission

In the case of coherent JT, APs cooperate by transmitting the same data to each user in a synchronous manner, resembling a distributed LED array. As a result, the received signals are combined in amplitude, rather than in power. The achieved SINR at the typical user under the coherent JT scheme can be formulated as:

$$\mathrm{SINR} = \frac{\left(\sum\limits_{x_i \in \Phi_{\mathrm{a}} \cap b(\mathrm{o}, D)} \left(x_i^2 + L^2 \right)^{-\frac{m+3}{2}} \right)^2}{\sum\limits_{x_i \in \Phi_{\mathrm{a}} \cap \bar{b}(\mathrm{o}, D)} \left(x_i^2 + L^2 \right)^{-(m+3)} + \bar{\sigma}_{\mathrm{n}}^2}. \qquad (7)$$

Note that the expressions for the SINR under noncoherent JT and coherent JT schemes are different only in the received signal power. Comparing (6) with (7), it is evident that coherent JT outperforms noncoherent JT in terms of the SINR since the numerator of (7) is greater than that of (6).

3 COVERAGE PROBABILITY ANALYSIS

In this section, we focus on the analysis of the coverage probability of a typical user in the network. The coverage probability is defined as the probability that the received SINR exceeds a certain threshold T. For both noncoherent and coherent JT schemes, the SINR expression can be written as:

$$\mathrm{SINR} = \frac{S}{I + \bar{\sigma}_{\mathrm{n}}^2}, \qquad (8)$$

where S and I represent the normalized received signal power and the normalized interference power at the typical user, respectively. Note that the normalization is to simplify the mathematical derivations. For example, S (I) represent the received signal (interference) power per transmit power, scaled by the distance-irrelevant fading parameter α^2. For noncoherent JT, $S = \sum_{x_i \in \Phi_{\mathrm{a}} \cap b(\mathrm{o}, D)} \left(x_i^2 + L^2 \right)^{-(m+3)}$, while for coherent JT, $S = \left(\sum_{x_i \in \Phi_{\mathrm{a}} \cap b(\mathrm{o}, D)} \left(x_i^2 + L^2 \right)^{-(m+3)/2} \right)^2$. For both noncoherent and coherent JT schemes, $I = \sum_{x_i \in \Phi_{\mathrm{a}} \cap \bar{b}(\mathrm{o}, D)} \left(x_i^2 + L^2 \right)^{-(m+3)}$. Since S and I are functions of points located in two disjoint sets of the PPP, they are statistically independent. Therefore, the density function of the SINR can be obtained by studying the distribution functions of S and I separately.

3.1 Characteristic Functions of S and I

For noncoherent JT, the exact probability density functions (PDFs) of S and I can be obtained from the inversion of their characteristic functions [27]. More specifically, the characteristic function of S can be calculated as:

$$\begin{aligned}
\mathcal{F}_S(\omega) &= \mathbb{E}_{\Phi_{\mathrm{a}}}\left[\exp\left(j\omega S \right) \right] \\
&= \mathbb{E}_n\left[\mathbb{E}_{\Phi_{\mathrm{a}}}\left[\exp\left(j\omega S \right) \middle| \Phi_{\mathrm{a}}(b(\mathrm{o}, D)) = n \right] \right] \\
&= \sum_{n=0}^{\infty} \mathbb{P}\left[\sum_{x_i \in \Phi_{\mathrm{a}}} \mathbf{1}_{b(\mathrm{o}, D)}(x_i) = n \right] \\
&\quad \times \mathbb{E}_{\Phi_{\mathrm{a}}}\left[\prod_{x_i \in \Phi_{\mathrm{a}} \cap b(\mathrm{o}, D)} \exp\left(j\omega \left(x_i^2 + L^2 \right)^{-(m+3)} \right) \middle| \Phi_{\mathrm{a}}(b(\mathrm{o}, D)) = n \right] \\
&= \sum_{n=0}^{\infty} \frac{\left(\pi \lambda_{\mathrm{a}} D^2 \right)^n}{n!} \exp\left(-\pi \lambda_{\mathrm{a}} D^2 \right) \\
&\quad \times \left(\int_0^D f_{x \in b(\mathrm{o}, D)}(x) \exp\left(j\omega \left(x^2 + L^2 \right)^{-(m+3)} \right) \mathrm{d}x \right)^n, \qquad (9)
\end{aligned}$$

where $j = \sqrt{-1}$ and $f_{x \in b(\mathrm{o}, D)}(x)$ is the PDF of the distance of a point uniformly distributed inside ball $b(\mathrm{o}, D)$ to the origin. In the derivation of (9), the last step follows from the property of PPP, stating that the n points inside the set $\Phi_{\mathrm{a}} \cap b(\mathrm{o}, D)$ are independent. Due to the homogeneity of the PPP, we have $f_{x \in b(\mathrm{o}, D)}(x) = 2x/D^2$ for $x \leq D$, and zero otherwise. By reversely applying the Taylor series expansion, the characteristic function of S can be obtained as:

$$\begin{aligned}
&\mathcal{F}_S(\omega) \\
&= \exp\left(\pi \lambda_{\mathrm{a}} D^2 \left(\int_0^D \frac{2x}{D^2} \exp\left(j\omega \left(x^2 + L^2 \right)^{-(m+3)} \right) \mathrm{d}x - 1 \right) \right) \\
&= \exp\left\{ -\pi \lambda_{\mathrm{a}} D^2 + \frac{\pi \lambda_{\mathrm{a}}}{m+3} \left\{ -L^2 E_{\frac{m+4}{m+3}}\left(-j\omega L^{-2(m+3)} \right) \right. \right.
\end{aligned}$$

$$+ \left(D^2 + L^2 \right) E_{\frac{m+4}{m+3}} \left(-j\omega \left(D^2 + L^2 \right)^{-(m+3)} \right) \Bigg\} \Bigg\}, \qquad (10)$$

for $\omega \geq 0$, and $\mathcal{F}_S(\omega) = \mathcal{F}_S^*(-\omega)$ for $\omega < 0$. In (10), $E_n(z) = \int_1^\infty \exp(-zt)t^{-n}dt$ is the exponential integral function [28].

On the other hand, the characteristic function of the interference I can be calculated by following similar steps as (9):

$$\mathcal{F}_I(\omega)$$
$$= \sum_{n=0}^\infty \mathbb{P}\left[\sum_{x_i \in \Phi_a} \mathbf{1}_{\bar{b}(o,D)}(x_i) = n \right]$$
$$\times \mathbb{E}_{\Phi_a}\left[\prod_{x_i \in \Phi_a \cap \bar{b}(o,D)} \exp\left(j\omega \left(x_i^2 + L^2 \right)^{-(m+3)} \right) \Bigg| \Phi_a(\bar{b}(o,D)) = n \right]$$
$$= \sum_{n=0}^\infty \frac{\left(\lambda_a \mu(\bar{b}(o,D)) \right)^n}{n!} \exp\left(-\lambda_a \mu(\bar{b}(o,D)) \right)$$
$$\times \left(\int_D^\infty f_{x \in \bar{b}(o,D)}(x) \exp\left(j\omega \left(x^2 + L^2 \right)^{-(m+3)} \right) dx \right)^n, \qquad (11)$$

where $\mu(\bar{b}(o,D))$ is the standard Lebesgue measure of $\bar{b}(o,D)$, and $f_{x \in \bar{b}(o,D)}(x)$ is the PDF of the distance of a point uniformly distributed in $\bar{b}(o,D)$ to the origin. Since $\bar{b}(o,D)$ is an unbounded region, $\mathcal{F}_I(\omega)$ can be calculated by considering $\bar{b}(o,D)$ as an annulus with inner radius D and outer radius $D_o \to \infty$:

$$\mathcal{F}_I(\omega) = \lim_{D_o \to \infty} \sum_{n=0}^\infty \frac{\left(\pi\lambda_a \left(D_o^2 - D^2 \right) \right)^n}{n!} \exp\left(-\pi\lambda_a \left(D_o^2 - D^2 \right) \right)$$
$$\times \left(\int_D^{D_o} \frac{2x}{D_o^2 - D^2} \exp\left(j\omega \left(x^2 + L^2 \right)^{-(m+3)} \right) dx \right)^n$$
$$= \lim_{D_o \to \infty} \exp\left\{ \pi\lambda_a \left(D_o^2 - D^2 \right) \left\{ \int_D^{D_o} \frac{2x}{D_o^2 - D^2} \right. \right.$$
$$\left. \left. \times \exp\left(j\omega \left(x^2 + L^2 \right)^{-(m+3)} \right) dx - 1 \right\} \right\}. \qquad (12)$$

Using a change of variable $t = \left(x^2 + L^2 \right)^{-(m+3)}$ and integration by parts, $\mathcal{F}_I(\omega)$ can be further simplified to:

$$\mathcal{F}_I(\omega)$$
$$= \exp\left(\pi\lambda_a j\omega \int_0^{(D^2+L^2)^{-(m+3)}} \left(t^{-\frac{1}{m+3}} - D^2 - L^2 \right) \exp\left(j\omega t \right) dt \right)$$
$$= \exp\left\{ \pi\lambda_a \left(D^2 + L^2 \right) \left(1 - \exp\left(j\omega \left(D^2 + L^2 \right)^{-(m+3)} \right) \right) \right.$$
$$+ \pi\lambda_a (-j\omega)^{\frac{1}{m+3}} \Gamma\left(\frac{m+2}{m+3}, -j\omega \left(D^2 + L^2 \right)^{-(m+3)} \right)$$
$$\left. - \pi\lambda_a (-j\omega)^{\frac{1}{m+3}} \Gamma\left(\frac{m+2}{m+3} \right) \right\}, \qquad (13)$$

for $\omega \geq 0$, and $\mathcal{F}_I(\omega) = \mathcal{F}_I^*(-\omega)$ for $\omega < 0$. In (13), $\Gamma(z) = \int_0^\infty \exp(-t)t^{z-1}dt$ is the standard gamma function and $\Gamma(n,z) = \int_z^\infty \exp(-t)t^{n-1}dt$ is the upper incomplete gamma function [28].

As can be seen from (10) and (13), the characteristic functions $\mathcal{F}_S(\omega)$ and $\mathcal{F}_I(\omega)$ are both in complicated forms, and no explicit expressions are available for the PDFs of S and I. Therefore, numerical methods are required for the
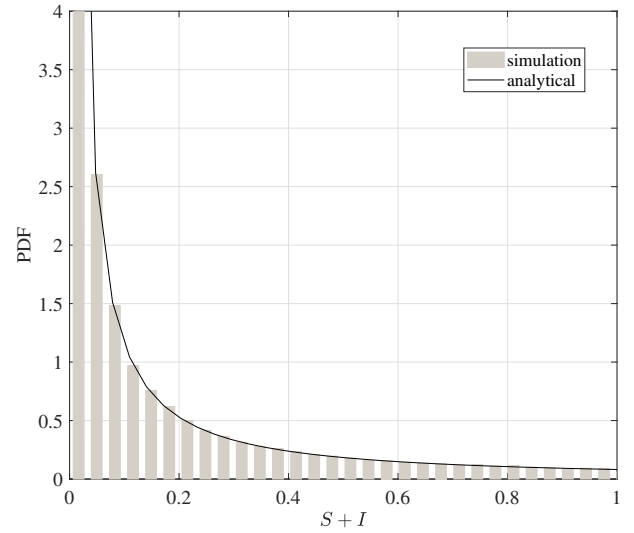

Fig. 2. The PDF of $S + I$ for noncoherent JT. The parameters are $\Psi_{1/2} = 60°$, $\lambda_a = 0.1$ and $L = 1$ m. The empirical data is obtained from $80,000$ realizations while the analytical expression is calculated from (14) by summing the first 100 terms.

calculation of PDFs of S and I. This can be achieved by performing the inverse Fourier transform or using the Gram-Charlier series expansion with infinite terms and Laguerre polynomials [29]. However, these two approaches are not pursued here due to their high computation complexity and the lack of insights into the distribution characteristics of S and I.

We point out here that, for noncoherent JT, an analytical expression for the PDF of $S + I$ is available, which is given in the following proposition.

Proposition 1. The PDF of $S + I$ for noncoherent JT is:

$$f_{S+I}(t) = \frac{1}{\pi t} \exp\left(\pi\lambda_a L^2 \right) \sum_{n=1}^\infty \frac{\Gamma\left(\frac{n}{m+3} + 1 \right)}{n!}$$
$$\times \left(\pi\lambda_a \Gamma\left(\frac{m+2}{m+3} \right) t^{-\frac{1}{m+3}} \right)^n \sin\left(\frac{m+2}{m+3} n\pi \right). \qquad (14)$$

Proof: The characteristic function of $S + I$ for noncoherent JT can treated as a special case of $\mathcal{F}_S(\omega)$ when $D \to \infty$. Therefore, it can be obtained from:

$$\mathcal{F}_{S+I}(\omega) = \lim_{D \to \infty} \mathcal{F}_S(\omega)$$
$$= \exp\left(\pi\lambda_a j\omega \int_0^\infty \left(t^{-\frac{1}{m+3}} - L^2 \right) \exp\left(j\omega t \right) dt \right)$$
$$= \exp\left(-\pi\lambda_a \left(\Gamma\left(\frac{m+2}{m+3} \right) (-j\omega)^{\frac{1}{m+3}} - L^2 \right) \right), \qquad (15)$$

in which the second step follows from a change of variable $t = \left(x^2 + L^2 \right)^{-(m+3)}$ and integration by parts. The inverse Fourier transform of $\mathcal{F}_{S+I}(\omega)$ gives the PDF of $S + I$. Since it satisfies that $0 < 1/(m+3) < 1$, (14) can be readily obtained by following similar procedures as described in [27]. □

In Fig. 2, the analytical expression in (14) is compared with the empirical PDF of $S + I$ obtained from Monte Carlo simulations. It can be seen that the derived analytical expression closely matches the simulation results. However, the exact distribution functions of S and I are difficult to obtain from their characteristic functions. In the following,

we resort to finding approximate distributions of S and I for both noncoherent JT and coherent JT schemes.

3.2 Noncoherent Joint Transmission

In this subsection, approximate distribution functions of S and I for noncoherent JT are derived through second-order moment matching. Since S and I are two independent variables, the PDFs of S and I are sufficient for the coverage probability characterization.

Proposition 2. The normalized signal power S for noncoherent JT can be accurately approximated by a gamma distribution, whose shape parameter k_S and scale parameter θ_S are given by:

$$k_S = \pi \lambda_a \frac{2m+5}{(m+2)^2} \frac{\left(L^{-2(m+2)} - \left(D^2 + L^2\right)^{-(m+2)}\right)^2}{L^{-2(2m+5)} - \left(D^2 + L^2\right)^{-(2m+5)}}, \quad (16)$$

$$\theta_S = \frac{m+2}{2m+5} \frac{L^{-2(2m+5)} - \left(D^2 + L^2\right)^{-(2m+5)}}{L^{-2(m+2)} - \left(D^2 + L^2\right)^{-(m+2)}}. \quad (17)$$

Proof: The parameterization of k_S and θ_S can be obtained by matching the first order (mean) and second order (variance) moments of the gamma distribution. The mean of S can be calculated from the Campbell's theorem [11]:

$$\mathbb{E}[S] = \mathbb{E}\left[\sum_{x_i \in \Phi_a \cap b(o,D)} \left(x_i^2 + L^2\right)^{-(m+3)}\right]$$
$$= 2\pi \lambda_a \int_0^D x \left(x^2 + L^2\right)^{-(m+3)} dx$$
$$= \frac{\pi \lambda_a}{m+2} \left(L^{-2(m+2)} - \left(D^2 + L^2\right)^{-(m+2)}\right). \quad (18)$$

Similarly, the variance of S can be calculated as:

$$\text{Var}[S] = \mathbb{E}\left[S^2\right] - (\mathbb{E}[S])^2$$
$$= \mathbb{E}\left[\sum_{x_i \in \Phi_a \cap b(o,D)} \left(x_i^2 + L^2\right)^{-2(m+3)}\right]$$
$$= 2\pi \lambda_a \int_0^D x \left(x^2 + L^2\right)^{-2(m+3)} dx$$
$$= \frac{\pi \lambda_a}{2m+5} \left(L^{-2(2m+5)} - \left(D^2 + L^2\right)^{-(2m+5)}\right), \quad (19)$$

where the second step follows from [30, Corollary 4.8]. Since a gamma distribution with shape parameter k_S and scale parameter θ_S has mean $k_S \theta_S$ and variance $k_S \theta_S^2$, k_S and θ_S can be obtained from $k_S = (\mathbb{E}[S])^2 / \text{Var}[S]$ and $\theta_S = \text{Var}[S]/\mathbb{E}[S]$, respectively. □

Based on Proposition 2, the approximate PDF of S for noncoherent JT can therefore be written as:

$$f_S(S) \approx \frac{\theta_S^{-k_S}}{\Gamma(k_S)} S^{k_S - 1} \exp\left(-\frac{S}{\theta_S}\right). \quad (20)$$

Proposition 3. The normalized interference I for noncoherent JT can be accurately approximated by a gamma dis-

tribution, whose shape parameter k_I and scale parameter θ_I are given by:

$$k_I = \pi \lambda_a \frac{2m+5}{(m+2)^2} \frac{\left(D^2 + L^2\right)^{-2(m+2)}}{\left(D^2 + L^2\right)^{-(2m+5)}}, \quad (21)$$

$$\theta_I = \frac{m+2}{2m+5} \frac{\left(D^2 + L^2\right)^{-(2m+5)}}{\left(D^2 + L^2\right)^{-(m+2)}}. \quad (22)$$

Proof: The proof is similar to that of Proposition 2, using the following expressions for the mean and variance of I:

$$\mathbb{E}[I] = \frac{\pi \lambda_a}{m+2} \left(D^2 + L^2\right)^{-(m+2)}, \quad (23)$$

$$\text{Var}[I] = \frac{\pi \lambda_a}{2m+5} \left(D^2 + L^2\right)^{-(2m+5)}. \quad (24)$$

Similarly, k_I and θ_I can be obtained from $k_I = (\mathbb{E}[I])^2 / \text{Var}[I]$ and $\theta_I = \text{Var}[I]/\mathbb{E}[I]$, respectively. □

Based on Proposition 3, the approximate PDF of I for noncoherent JT can therefore be written as:

$$f_I(I) \approx \frac{\theta_I^{-k_I}}{\Gamma(k_I)} I^{k_I - 1} \exp\left(-\frac{I}{\theta_I}\right). \quad (25)$$

By approximating the signal power and interference as two independent gamma distributions, a tractable analytical expression for the coverage probability can be derived. As will be shown in the simulation results, despite being simple, such approximations can provide accurate results for calculating the coverage probability.

Theorem 1. For noncoherent JT, the coverage probability of a typical user can be well approximated by:

$$\mathbb{P}[\text{SINR} > T] \approx 1 - \frac{\theta_I^{-k_I}}{\Gamma(k_S)} \sum_{n=0}^{\infty} \frac{(-1)^n}{n!(k_S + n)} \left(\frac{T}{\theta_S}\right)^{k_S + n}$$
$$\times \left(\bar{\sigma}_n^2\right)^{k_S + k_I + n} U\left(k_I, k_S + k_I + n + 1, \frac{\bar{\sigma}_n^2}{\theta_I}\right), \quad (26)$$

where k_S, θ_S, k_I and θ_I are given in (16), (17), (21) and (22), respectively, and $U(a, b, z) = \Gamma^{-1}(a) \int_0^{\infty} \exp(-zt) t^{a-1} (1+t)^{b-a-1} dt$ is the confluent hypergeometric function [28].

Proof: Starting with Proposition 2 and Proposition 3, the coverage probability can be calculated using properties of the gamma distribution:

$$\mathbb{P}[\text{SINR} > T]$$
$$= \mathbb{E}_I\left[\mathbb{P}\left[S > T\left(I + \bar{\sigma}_n^2\right)\Big| I\right]\right]$$
$$\approx \mathbb{E}_I\left[\frac{\Gamma\left(k_S, \frac{T(I + \bar{\sigma}_n^2)}{\theta_S}\right)}{\Gamma(k_S)}\right]$$
$$\approx \frac{\theta_I^{-k_I}}{\Gamma(k_S)\Gamma(k_I)} \int_0^{\infty} I^{k_I - 1} \exp\left(-\frac{I}{\theta_I}\right) \Gamma\left(k_S, \frac{T(I + \bar{\sigma}_n^2)}{\theta_S}\right) dI, \quad (27)$$

where the second step is based on (20) and the last step is obtained with the insertion of (25). Using the series

expansion of the upper incomplete gamma function [28, Eq. 8.354.2], (27) can be rewritten as:

$$\mathbb{P}[\text{SINR} > T] \approx \frac{\theta_I^{-k_I}}{\Gamma(k_S)\Gamma(k_I)} \int_0^\infty I^{k_I-1} \exp\left(-\frac{I}{\theta_I}\right)$$
$$\times \left(\Gamma(k_S) - \sum_{n=0}^\infty \frac{(-1)^n \left(\frac{T(I+\bar{\sigma}_n^2)}{\theta_S}\right)^{k_S+n}}{n!(k_S+n)}\right) dI$$
$$= 1 - \frac{\theta_I^{-k_I}}{\Gamma(k_S)\Gamma(k_I)} \sum_{n=0}^\infty \frac{(-1)^n}{n!(k_S+n)}$$
$$\times \int_0^\infty I^{k_I-1} \exp\left(-\frac{I}{\theta_I}\right) \left(\frac{T(I+\bar{\sigma}_n^2)}{\theta_S}\right)^{k_S+n} dI. \tag{28}$$

With a change of variable $t = I/\bar{\sigma}_n^2$, (28) can be further simplified into:

$$\mathbb{P}[\text{SINR} > T]$$
$$\approx 1 - \frac{\theta_I^{-k_I}}{\Gamma(k_S)\Gamma(k_I)} \sum_{n=0}^\infty \frac{(-1)^n}{n!(k_S+n)} \left(\frac{T}{\theta_S}\right)^{k_S+n} \left(\bar{\sigma}_n^2\right)^{k_S+k_I+n}$$
$$\times \int_0^\infty t^{k_I-1} \exp\left(-\frac{\bar{\sigma}_n^2}{\theta_I}t\right)(1+t)^{k_S+n} dt. \tag{29}$$

Applying [28, Eq. 9.211.4], the integration in (29) can be interpreted as the integral representation of the confluent hypergeometric function with parameters k_I, $k_S + k_I + n + 1$ and $\bar{\sigma}_n^2/\theta_I$. After further simplifications, the coverage probability can be obtained as shown in (26). □

The result presented in Theorem 1 is applicable for the coverage probability calculation with arbitrary network parameters. Nevertheless, significant simplification is possible if the communication link is interference-limited, i.e., $\bar{\sigma}_n^2 = 0$. We present this result in the following proposition.

Proposition 4. For noncoherent JT, the coverage probability of a typical user in the interference-limited region can be approximated by:

$$\mathbb{P}[\text{SINR} > T]$$
$$\approx \frac{\Gamma(k_S+k_I)}{k_I \Gamma(k_S)\Gamma(k_I)} \left(\frac{\theta_S}{\theta_I T}\right)^{k_I} {}_2F_1\left(k_I, k_S+k_I; k_I+1; -\frac{\theta_S}{\theta_I T}\right), \tag{30}$$

where ${}_2F_1(\cdot, \cdot; \cdot; \cdot)$ is the Gauss hypergeometric function [28].

Proof: Starting from (27), when $\bar{\sigma}_n^2 = 0$, the coverage probability can be simplified to:

$$\mathbb{P}[\text{SINR} > T]$$
$$\approx \frac{\theta_I^{-k_I}}{\Gamma(k_S)\Gamma(k_I)} \int_0^\infty I^{k_I-1} \exp\left(-\frac{I}{\theta_I}\right) \Gamma\left(k_S, \frac{TI}{\theta_S}\right) dI. \tag{31}$$

The integration in (31) can be further calculated as:

$$\int_0^\infty I^{k_I-1} \exp\left(-\frac{I}{\theta_I}\right) \Gamma\left(k_S, \frac{TI}{\theta_S}\right) dI$$
$$= \frac{\Gamma(k_S+k_I)\left(\frac{\theta_S}{T}\right)^{k_I}}{k_I\left(1+\frac{\theta_S}{\theta_I T}\right)^{k_S+k_I}} {}_2F_1\left(1, k_S+k_I; k_I+1; \frac{1}{1+\frac{\theta_I}{\theta_S}T}\right)$$
$$= \frac{\Gamma(k_S+k_I)}{k_I}\left(\frac{\theta_S}{T}\right)^{k_I} {}_2F_1\left(k_I, k_S+k_I; k_I+1; -\frac{\theta_S}{\theta_I T}\right), \tag{32}$$

where the first step follows from [28, Eq. 6.455.1] and the second step is obtained with the use of Pfaff transformation [28, Eq. 9.131.1]. Inserting (32) into (31) yields (30), which completes the proof. □

Notice that the coverage probability in (30) depends on k_S, k_I and the ratio between θ_S and θ_I. When the communication link is interference-limited, Proposition 4 provides a more tractable result than Theorem 1 for the coverage probability computation. For the general case when $\bar{\sigma}_n^2 \neq 0$, the coverage probability is more accurately characterized by Theorem 1, while Proposition 4 can be used as an analytical upper bound.

3.3 Coherent Joint Transmission

In this subsection, approximate distribution functions of S and I for coherent JT are derived using a similar method as the derivation for the case of noncoherent JT. Since the independence between S and I still preserves, the coverage probability can also be computed using the PDFs of S and I.

Remark 1. The normalized interference I for noncoherent JT and coherent JT are the same, so are their distributions. Therefore, for coherent JT, I can also be approximated by a gamma distribution with shape parameter k_I and scale parameter θ_I given by (21) and (22), respectively.

For coherent JT, the expression for S is given as a square of sum. As a result, the gamma distribution is no longer accurate for modeling the distribution of S.

Proposition 5. The signal power S for coherent JT can be accurately approximated by a generalized gamma distribution, whose PDF is:

$$f_S(S) \approx \frac{p_S}{a_S^{d_S}\Gamma\left(\frac{d_S}{p_S}\right)} S^{d_S-1} \exp\left(-\left(\frac{S}{a_S}\right)^{p_S}\right), \tag{33}$$

where the shape parameter a_S and two scale parameters d_S and p_S are given by:

$$a_S = \left(\frac{(m+1)}{2(m+2)}\frac{L^{-2(m+2)} - (D^2+L^2)^{-(m+2)}}{L^{-(m+1)} - (D^2+L^2)^{-\frac{m+1}{2}}}\right)^2, \tag{34}$$

$$d_S = 2\pi\lambda_a \frac{m+2}{(m+1)^2}\frac{\left(L^{-(m+1)} - (D^2+L^2)^{-\frac{m+1}{2}}\right)^2}{L^{-2(m+2)} - (D^2+L^2)^{-(m+2)}}, \tag{35}$$

$$p_S = \frac{1}{2}, \tag{36}$$

respectively.

Proof: We start by studying the distribution of the signal amplitude $Y = \sqrt{S} = \sum_{x_i \in \Phi_a \cap b(o,D)} \left(x_i^2 + L^2\right)^{-(m+3)/2}$.

Since Y for coherent JT has a similar expression as S for noncoherent JT, it can also be approximated by a gamma distribution. The mean and variance of Y are found to be:

$$\mathbb{E}[Y] = \frac{2\pi\lambda_a}{m+1}\left(L^{-(m+1)} - \left(D^2 + L^2\right)^{-\frac{m+1}{2}}\right), \quad (37)$$

$$\mathrm{Var}[Y] = \frac{\pi\lambda_a}{m+2}\left(L^{-2(m+2)} - \left(D^2 + L^2\right)^{-(m+2)}\right). \quad (38)$$

By letting $\mathbb{E}[Y] = k_Y\theta_Y$ and $\mathrm{Var}[Y] = k_Y\theta_Y^2$, we obtain the shape parameter k_Y and scale parameter θ_Y for the gamma distribution of Y:

$$k_Y = 4\pi\lambda_a \frac{m+2}{(m+1)^2}\frac{\left(L^{-(m+1)} - \left(D^2 + L^2\right)^{-\frac{m+1}{2}}\right)^2}{L^{-2(m+2)} - \left(D^2 + L^2\right)^{-(m+2)}}, \quad (39)$$

$$\theta_Y = \frac{(m+1)}{2(m+2)}\frac{L^{-2(m+2)} - \left(D^2 + L^2\right)^{-(m+2)}}{L^{-(m+1)} - \left(D^2 + L^2\right)^{-\frac{m+1}{2}}}. \quad (40)$$

Based on the property of gamma distribution, the cumulative distribution function (CDF) of S can be obtained as:

$$\mathbb{P}[S < t] = \mathbb{P}\left[Y < \sqrt{t}\right] \approx 1 - \frac{\Gamma\left(k_Y, \frac{\sqrt{t}}{\theta_Y}\right)}{\Gamma(k_Y)}. \quad (41)$$

Calculating derivative of the CDF yields the PDF of S:

$$f_S(t) = \frac{\partial}{\partial t}\mathbb{P}[S < t] \approx \frac{\theta_Y^{-k_Y}}{2\Gamma(k_Y)}t^{\frac{k_Y}{2}-1}\exp\left(-\frac{\sqrt{t}}{\theta_Y}\right), \quad (42)$$

which falls into the category of generalized gamma distribution, whose scale parameter and two shape parameters are $a_S = \theta_Y^2$, $p_S = k_Y/2$ and $d_S = 1/2$, respectively. □

With the signal power being modeled as a generalized gamma distribution and the interference power being modeled as a gamma distribution, a tractable analytical expression for the coverage probability is given in the following theorem.

Theorem 2. For coherent JT, the coverage probability of a typical user can be well approximated by:

$$\mathbb{P}[\mathsf{SINR} > T] \approx 1 - \frac{\theta_I^{-k_I}}{\Gamma(k_Y)}\sum_{n=0}^{\infty}\frac{(-1)^n}{n!(k_Y+n)}\left(\bar{\sigma}_n^2\right)^{\frac{k_Y}{2}+k_I+\frac{n}{2}}$$
$$\times \left(\frac{\sqrt{T}}{\theta_Y}\right)^{k_S+n} U\left(k_I, \frac{k_Y}{2}+k_I+\frac{n}{2}+1, \frac{\bar{\sigma}_n^2}{\theta_I}\right), \quad (43)$$

where k_Y, θ_Y, k_I and θ_I are given in (39), (40), (21) and (22), respectively.

Proof: According to Proposition 3 and Proposition 5, the coverage probability can be calculated using properties of the generalized gamma distribution of S and the gamma distribution of I:

$$\mathbb{P}[\mathsf{SINR} > T]$$
$$= \mathbb{E}_I\left[\mathbb{P}\left[S > T\left(I + \bar{\sigma}_n^2\right)\Big| I\right]\right]$$
$$\approx \mathbb{E}_I\left[\frac{\Gamma\left(\frac{d_S}{p_S}, \left(\frac{T(I+\bar{\sigma}_n^2)}{a_S}\right)^{p_S}\right)}{\Gamma(k_Y)}\right]$$
$$\approx \frac{\theta_I^{-k_I}}{\Gamma(k_Y)\Gamma(k_I)}\int_0^\infty I^{k_I-1}\exp\left(-\frac{I}{\theta_I}\right)\Gamma\left(k_Y, \frac{\sqrt{T(I+\bar{\sigma}_n^2)}}{\theta_Y}\right)dI, \quad (44)$$

where the second step is based on (33) and the last is from the insertion of (25). By following similar steps as in (28) and (29), (43) can be obtained. □

Note that the coverage probability derived in Theorem 2 is generally applicable for arbitrary network parameters. Nevertheless, the result can be further simplified if the communication link is interference-limited. This simplified result is given in the following proposition.

Proposition 6. For coherent JT, the coverage probability of a typical user in the interference-limited region can be approximated by:

$$\mathbb{P}[\mathsf{SINR} > T]$$
$$\approx 1 + \frac{1}{\Gamma(k_Y)\Gamma(k_I)}\left(\frac{\sqrt{\theta_I T}}{\theta_Y}\right)^{k_Y}\left\{\frac{\sqrt{\theta_I T}\Gamma\left(\frac{k_Y}{2}+k_I+\frac{1}{2}\right)}{\theta_Y(k_Y+1)}\right.$$
$$\times {}_2F_2\left(\frac{k_Y+1}{2}, \frac{k_Y}{2}+k_I+\frac{1}{2}; \frac{3}{2}, \frac{k_Y+3}{2}; \frac{\theta_I T}{4\theta_Y^2}\right)$$
$$\left. -\frac{\Gamma\left(\frac{k_Y}{2}+k_I\right)}{k_Y}{}_2F_2\left(\frac{k_Y}{2}+k_I, \frac{k_Y}{2}; \frac{1}{2}, \frac{k_Y}{2}+1; \frac{\theta_I T}{4\theta_Y^2}\right)\right\}, \quad (45)$$

where ${}_2F_2(\cdot, \cdot; \cdot, \cdot; \cdot)$ is the generalized hypergeometric series [28].

Proof: Starting from (44), when $\bar{\sigma}_n^2 = 0$, the coverage probability can be simplified using a change of variable $t = \sqrt{TI}/\theta_Y$:

$$\mathbb{P}[\mathsf{SINR} > T]$$
$$\approx \frac{\theta_I^{-k_I}}{\Gamma(k_Y)\Gamma(k_I)}\int_0^\infty I^{k_I-1}\exp\left(-\frac{I}{\theta_I}\right)\Gamma\left(k_Y, \frac{\sqrt{TI}}{\theta_Y}\right)dI$$
$$= \frac{2}{\Gamma(k_Y)\Gamma(k_I)}\left(\frac{\theta_Y^2}{\theta_I T}\right)^{k_I}\int_0^\infty t^{2k_I-1}\exp\left(-\frac{\theta_Y^2}{\theta_I T}t^2\right)\Gamma(k_Y, t)dt. \quad (46)$$

After replacing the incomplete gamma function in (46) with a series representation [28, Eq. 8.354.2], the coverage proba-

bility can be expressed as:

$$
\mathbb{P}\left[\mathsf{SINR} > T\right]
$$

$$
\approx \frac{2}{\Gamma(k_Y)\Gamma(k_I)}\left(\frac{\theta_Y^2}{\theta_I T}\right)^{k_I}\int_0^\infty t^{2k_I-1}\exp\left(-\frac{\theta_Y^2}{\theta_I T}t^2\right)
$$

$$
\times\left(\Gamma(k_Y)-\sum_{n=0}^\infty\frac{(-1)^n}{n!(k_Y+n)}t^{k_Y+n}\right)\mathrm{d}t
$$

$$
=1-\frac{2}{\Gamma(k_Y)\Gamma(k_I)}\left(\frac{\theta_Y^2}{\theta_I T}\right)^{k_I}\sum_{n=0}^\infty\frac{(-1)^n}{n!(k_Y+n)}
$$

$$
\times\int_0^\infty t^{k_Y+2k_I+n-1}\exp\left(-\frac{\theta_Y^2}{\theta_I T}t^2\right)\mathrm{d}t
$$

$$
=1-\frac{1}{\Gamma(k_Y)\Gamma(k_I)}\left(\frac{\sqrt{\theta_I T}}{\theta_Y}\right)^{k_Y}\sum_{n=0}^\infty\frac{(-1)^n}{n!(k_Y+n)}\left(\frac{\theta_I T}{\theta_Y^2}\right)^{\frac{n}{2}}
$$

$$
\times\Gamma\left(\frac{k_Y}{2}+k_I+\frac{n}{2}\right). \tag{47}
$$

Interpreting the sum of infinites series as two sums with odd and even indexes, (47) can be rewritten as:

$$
\mathbb{P}\left[\mathsf{SINR} > T\right]\approx 1+\frac{1}{\Gamma(k_Y)\Gamma(k_I)}\left(\frac{\sqrt{\theta_I T}}{\theta_Y}\right)^{k_Y}\left\{\sum_{n=0}^\infty\left(\frac{\theta_I T}{\theta_Y^2}\right)^{n+\frac{1}{2}}\right.
$$

$$
\times\frac{\Gamma\left(\frac{k_Y}{2}+k_I+n+\frac{1}{2}\right)}{(2n+1)!(k_Y+2n+1)}-\sum_{n=0}^\infty\left(\frac{\theta_I T}{\theta_Y^2}\right)^n\frac{\Gamma\left(\frac{k_Y}{2}+k_I+n\right)}{(2n)!(k_Y+2n)}\right\}. \tag{48}
$$

Based on the identities $(2n)! = n!4^n\Gamma(n+1/2)/\Gamma(1/2)$ and $(2n+1)! = 2(n)!4^n\Gamma(n+3/2)/\Gamma(1/2)$, we have:

$$
\mathbb{P}\left[\mathsf{SINR} > T\right]\approx 1+\frac{1}{\Gamma(k_Y)\Gamma(k_I)}\left(\frac{\sqrt{\theta_I T}}{\theta_Y}\right)^{k_Y}\sum_{n=0}^\infty\frac{\Gamma\left(\frac{1}{2}\right)}{2\Gamma\left(n+\frac{1}{2}\right)}\frac{1}{n!}
$$

$$
\times\left(\frac{\theta_I T}{4\theta_Y^2}\right)^n\left(\frac{\sqrt{\theta_I T}}{\theta_Y}\frac{\Gamma\left(\frac{k_Y}{2}+k_I+n+\frac{1}{2}\right)}{2\left(n+\frac{1}{2}\right)\left(\frac{k_Y}{2}+n+\frac{1}{2}\right)}-\frac{\Gamma\left(\frac{k_Y}{2}+k_I+n\right)}{\frac{k_Y}{2}+n}\right). \tag{49}
$$

Interpreting the infinite series in (49) as the generalized hypergeometric series, we obtain, after some simplification, the expression for the coverage probability shown in (45). □

It can be seen that the coverage probability in (45) depends on k_Y, k_I and the ratio between $\sqrt{\theta_I}$ and θ_Y. When the communication link is dominated by interference, evaluating the coverage probability using Proposition 6 is more analytically tractable than using Theorem 2. For the general case when $\bar{\sigma}_n^2 \neq 0$, the coverage probability can be more accurately computed with Theorem 2, while Proposition 6 serves as an analytical upper bound.

4 SIMULATION RESULTS

In this section, Monte Carlo simulation results are presented to validate the theoretical results derived in Section 3. For the simulation setup, we consider an indoor office of size $18\times 14\times 3.5$ m^3, as depicted in Fig. 1. If not otherwise specified, the following parameters are assumed. The VLC APs have a semi-angle of $60°$, and all active APs transmit at
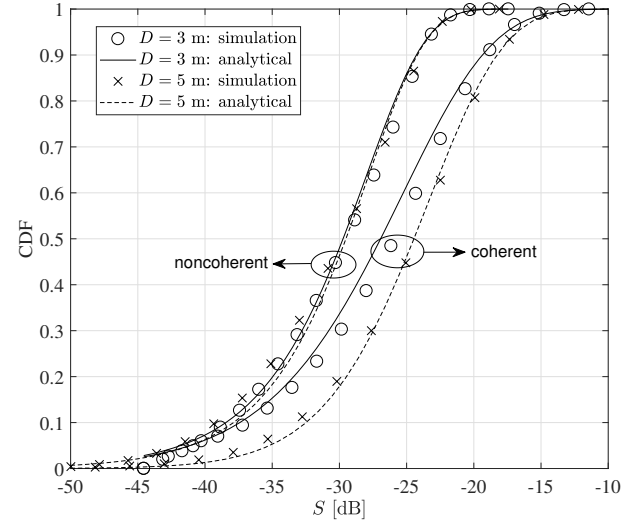

Fig. 3. The empirical and approximate CDFs of the normalized signal power S.

the same power level, which is 1 W [2], [25]. The PD used at the receiver side has a FOV of $90°$, an effective detection area of 1 cm^2, and a responsivity of 0.4 A/W [24], [25]. The vertical separation between users and VLC APs is set to 2 m. The VLC modulation bandwidth and the receiver noise power density are assumed to be 20 MHz and 10^{-22} A^2/Hz, respectively [2], [25]. This determines a typical value of the receiver noise power, that is −117.0 dBm. At the receiver front end, we assume that the optical concentrator has a reflective index of 1.5, and the optical filter has a unity gain [2]. The density of interfering APs is assumed to be 0.1.

Fig. 3 compares the approximate CDF of the normalized signal power with its empirical CDF obtained through simulations. It can be seen that for noncoherent JT, the signal power is well modeled by the gamma distribution (Proposition 2). For coherent JT, the signal power is well approximated by the generalized gamma distribution (Proposition 5). When the cooperation radius increases from 3 m to 5 m, only a slight improvement on the received signal power is observed for noncoherent JT. This is because signals transmitted from APs that are further away from the user are more severely attenuated. However, for coherent JT, signals transmitted by APs within the cooperation region are constructively added in amplitude. Therefore, when the cooperation radius for coherent JT is expanded from 3 m to 5 m, $2-5$ dB improvement on the normalized signal power is observed. Fig. 3 also shows that coherent JT outperforms its noncoherent counterpart in terms of the received signal power, but it requires more stringent signal synchronization and has higher implementation cost.

In Fig. 4, the empirical and approximate CDFs of the normalized interference power are compared. Since the interference has the same expression for both JT schemes, it is not explicitly distinguished in this context. It is shown in Fig. 4 that the gamma approximation of the interference power is reasonably accurate, with only slight deviations in the lower tail. As the cooperation radius is expanded from 3 m to 5 m, the normalized interference power is
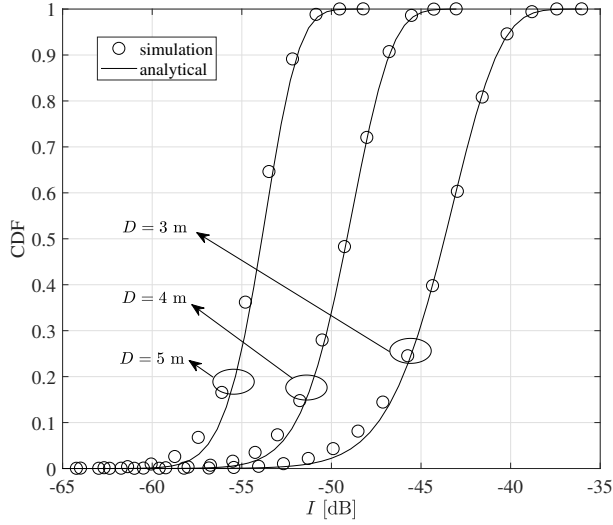
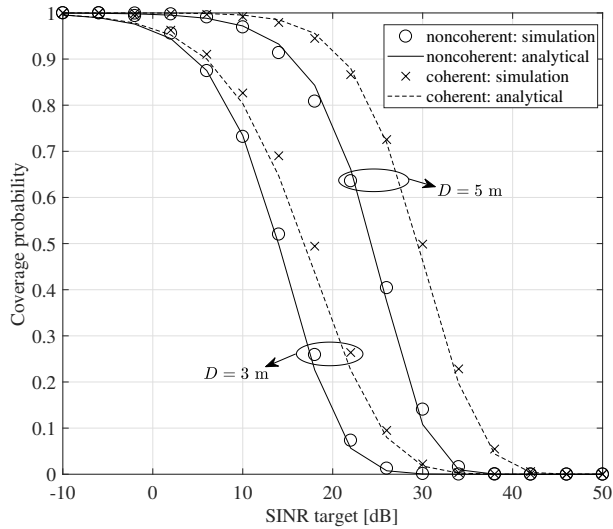Fig. 4. The empirical and approximate CDFs of the normalized interference power I.

Fig. 6. Coverage probabilities for noncoherent and coherent JT schemes with different sizes of the cooperation region ($T = 20$ dB).

Fig. 5. The comparison of coverage probabilities for noncoherent and coherent JT schemes.

Fig. 7. Coverage probabilities for noncoherent and coherent JT schemes with different densities of APs ($D = 3$ m).

reduced by 8−10 dB. Therefore, combining the results shown in Figs. 3 and 4, we can conclude that the main benefit of increasing the cooperation radius resides in the reduction of the interference level, rather than in the enhancement of useful signal power.

With different values of the target SINR, the coverage probability for noncoherent and coherent JT schemes are compared in Fig. 5. It can be seen that for both JT schemes, the derived analytical results match quite well with simulation results. It is also observed that increasing the cooperation radius can significantly enhance the coverage probability of a typical user. For example, when the SINR target is 20 dB, increasing the cooperation radius from 3 m to 5 m helps improve the coverage probability from 0.15 to 0.76 for noncoherent JT and from 0.33 to 0.92 for coherent JT, respectively. Fig. 5 also shows that coherent JT always yields a higher coverage probability than noncoherent JT, due to the accumulation in signal amplitude rather than in signal power. Furthermore, the gap between the coverage
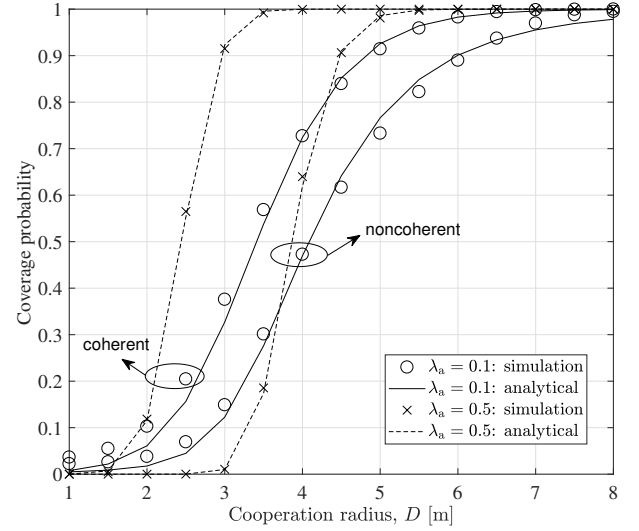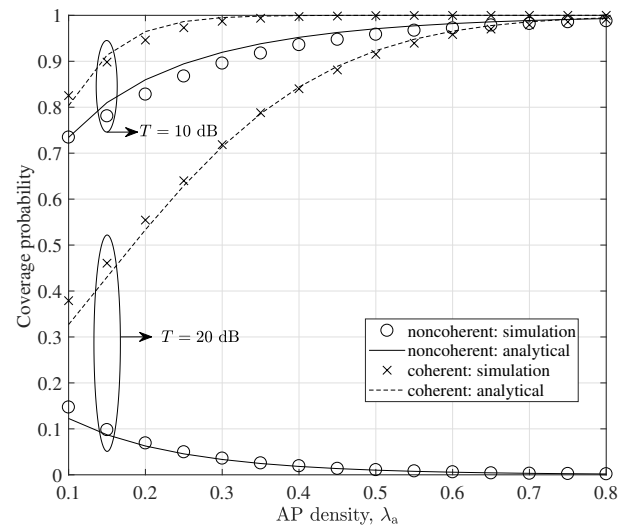
probabilities for noncoherent and coherent JT schemes enlarges as the the cooperation radius increases.

In Fig. 6, the coverage probabilities for noncoherent and coherent JT schemes are investigated with different sizes of the cooperation region. It is shown that for both JT schemes, the coverage probability increases as the cooperation radius increases. Notice that, on the one hand, when cooperation region is small, the coverage probability is higher when the density of APs is smaller. On the other hand, when cooperation region is large, the coverage probability is higher when the density of APs is larger. It is also shown that coherent JT gives a higher coverage probability than noncoherent JT, especially when the density of APs is large.

We investigate in Fig. 7 how the coverage probability of a typical user scales with the density of APs in the network. It can be seen that for a small value of the SINR target ($T = 10$ dB), the coverage probabilities for both JT schemes increase as the density of APs gets larger. However, for a
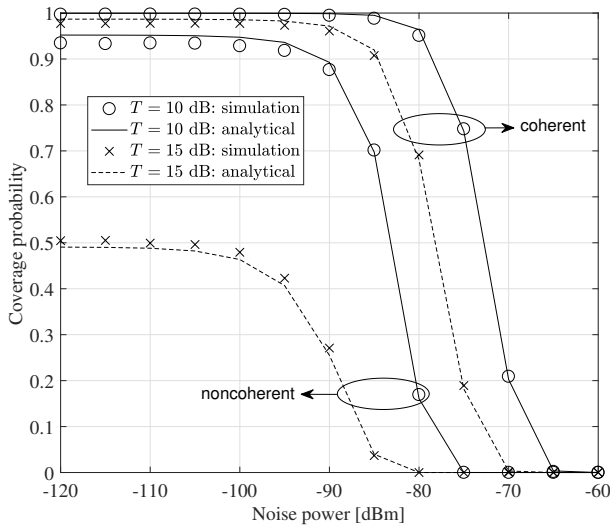
Fig. 8. The impact of receiver noise on the coverage probability for noncoherent and coherent JT schemes ($D = 3$ m, $\lambda_a = 0.4$).

large value of the SINR target ($T = 20$ dB), the coverage probabilities for both JT schemes scale differently with the density of APs. More specifically, the coverage probability for noncoherent JT monotonically decreases with an increase in the density of APs, while the coverage probability for coherent JT monotonically increases as the density of APs is increased. As a result, in comparison with noncoherent JT, the benefit of coherent JT becomes more significant when the target SINR is set at a higher value.

Since the derived analytical results are applicable with arbitrary receiver noise levels, we investigate in Fig. 8 the effect of receiver noise power on the coverage probability of a typical user. It can be seen from Fig. 8 that the analytical results are generally accurate across all receiver noise levels. For noise less than −110 dBm, the coverage probability remains constant because the communication link is interference-limited. As the noise power continues to increase, the coverage probability starts to decrease until it reaches zero. Therefore, for typical receiver noise of power −117.0 dBm [2], [25], assuming that the communication link is interference-limited is reasonable, and it can significantly simplify the coverage probability analysis for both noncoherent and coherent JT schemes (see Proposition 4 and Proposition 6).

5 CONCLUSIONS

In this paper, we presented a tractable model for the coverage analysis of multiuser VLC networks, taking into account the cooperation among APs. For both noncoherent JT and coherent JT, analytical expressions for the coverage probability have been derived and further simplified into closed forms when the communication link is interference-limited. The accuracy of the proposed analytical model has been validated through extensive Monte Carlo simulations. The performance of VLC networks has also been comprehensively investigated with various parameters. Results show that, although coherent JT requires more stringent signal synchronization and has higher implementation cost than noncoherent JT, it gives superior coverage performance to

users in the network, especially when the network is densely deployed with APs. Furthermore, the performance gain of coherent JT over its noncoherent counterpart is found to be more significant when the density of APs and the target SINR are increased. It is also shown that, for typical receiver noise levels, the SINR can be well approximated by the SIR to simplify the coverage analysis.

Throughout the paper, it is assumed that perfect CSI is available at both the transmitter and the receiver. In order to better understand the trade-offs and limitations of JT in practical VLC networks, future works taking into account the effect of imperfect CSI are of interest. Experimental evaluations of a practical VLC network are also worth investigating.

REFERENCES

[1] "Cisco visual networking index: Global mobile data traffic forecast update, 2016-2021," White Paper, Cisco, Mar. 2017.
[2] T. Komine and M. Nakagawa, "Fundamental analysis for visible-light communication system using LED lights," *IEEE Trans. Consum. Electron.*, vol. 50, no. 1, pp. 100–107, Feb. 2004.
[3] J. Grubor, S. Randel, K. D. Langer, and J. Walewski, "Broadband information broadcasting using LED-based interior lighting," *J. Lightw. Technol.*, vol. 26, no. 24, pp. 3883–3892, Dec. 2008.
[4] H. Haas, L. Yin, Y. Wang, and C. Chen, "What is LiFi?" *J. Lightw. Technol.*, vol. 34, no. 6, pp. 1533–1544, Mar. 2016.
[5] IEEE Std. 802.15.7-2011, *IEEE Standard for Local and Metropolitan Area Networks, Part 15.7: Short-Range Wireless Optical Communication Using Visible Light*, IEEE Std., 2011.
[6] H. Haas, "High-speed wireless networking using visible light," *SPIE Newsroom*, Apr. 2013.
[7] H. Ma, L. Lampe, and S. Hranilovic, "Coordinated broadcasting for multiuser indoor visible light communication systems," *IEEE Trans. Commun.*, vol. 63, no. 9, pp. 3313–3324, Sept. 2015.
[8] M. Kashef, M. Abdallah, K. Qaraqe, H. Haas, and M. Uysal, "Coordinated interference management for visible light communication systems," *J. Opt. Commun. Netw.*, vol. 7, no. 11, pp. 1098–1108, Nov. 2015.
[9] R. Zhang, J. Wang, Z. Wang, Z. Xu, C. Zhao, and L. Hanzo, "Visible light communications in heterogeneous networks: Paving the way for user-centric design," *IEEE Wireless Commun.*, vol. 22, no. 2, pp. 8–16, Apr. 2015.
[10] D. Bykhovsky and S. Arnon, "Multiple access resource allocation in visible light communication systems," *J. Lightw. Technol.*, vol. 32, no. 8, pp. 1594–1600, Feb. 2014.
[11] D. Stoyan, W. Kendall, and J. Mecke, *Stochastic Geometry and Its Applications*, 2nd ed. John Wiley and Sons, 1996.
[12] J. G. Andrews, F. Baccelli, and R. K. Ganti, "A tractable approach to coverage and rate in cellular networks," *IEEE Trans. Commun.*, vol. 59, no. 11, pp. 3122–3134, Nov. 2011.
[13] A. Baddeley, I. Bárány, R. Schneider, and W. Weil, *Stochastic Geometry*, ser. Lecture Notes in Mathematics. Springer-Verlag Berlin Heidelberg, 2007.
[14] H. ElSawy, A. Sultan-Salem, M.-S. Alouini, and M. Z. Win, "Modeling and analysis of cellular networks using stochastic geometry: A tutorial," *IEEE Commun. Surveys Tuts.*, vol. 19, no. 1, pp. 167–203, First Quarter 2017.
[15] C. Chen, D. A. Basnayaka, and H. Haas, "Downlink performance of optical attocell networks," *J. Lightw. Technol.*, vol. 34, no. 1, pp. 137–156, Jan. 2016.
[16] L. Yin and H. Haas, "Coverage analysis of multiuser visible light communication networks," *IEEE Trans. Wireless Commun.*, vol. 17, no. 3, pp. 1630–1643, Mar. 2017.

This article has been accepted for publication in a future issue of this journal, but has not been fully edited. Content may change prior to final publication. Citation information: DOI 10.1109/TMC.2018.2875687, IEEE Transactions on Mobile Computing

IEEE TRANSACTIONS ON MOBILE COMPUTING

12

[17] R. Irmer, H. Droste, P. Marsch, M. Grieger, G. Fettweis, S. Brueck, H.-P. Mayer, L. Thiele, and V. Jungnickel, "Coordinated multipoint: Concepts, performance, and field trial results," *IEEE Commun. Mag.*, vol. 49, no. 2, pp. 102–111, Feb. 2011.

[18] H. C. Ferreira, L. Lampe, J. Newbury, and T. G. Swart, Eds., *Power Line Communications: Theory and Applications for Narrowband and Broadband Communications over Power Lines*. Hoboken, NJ, USA: Wiley, 2010.

[19] T. Komine and M. Nakagawa, "Integrated system of white LED visible-light communication and power-line communication," *IEEE Trans. Consum. Electron.*, vol. 49, no. 1, pp. 71–79, 2003.

[20] H. Taoka, S. Nagata, K. Takeda, Y. Kakishima, X. She, and K. Kusume, "MIMO and CoMP in LTE-advanced," *NTT Docomo Tech. J.*, vol. 12, no. 2, pp. 20–28, Sept. 2010.

[21] D. Lee, H. Seo, B. Clerckx, E. Hardouin, D. Mazzarese, S. Nagata, and K. Sayana, "Coordinated multipoint transmission and reception in LTE-Advanced: Deployment scenarios and operational challenges," *IEEE Commun. Mag.*, vol. 50, no. 2, pp. 148–155, Feb. 2012.

[22] R. Tanbourgi, S. Singh, J. G. Andrews, and F. K. Jondral, "A tractable model for noncoherent joint-transmission base station cooperation," *IEEE Trans. Wireless Commun.*, vol. 13, no. 9, pp. 4959–4973, Sept. 2014.

[23] G. Nigam, P. Minero, and M. Haenggi, "Coordinated multipoint joint transmission in heterogeneous networks," *IEEE Trans. Commun.*, vol. 62, no. 11, pp. 4143–4146, Nov. 2014.

[24] J. Kahn and J. Barry, "Wireless infrared communications," *Proc. IEEE*, vol. 85, no. 2, pp. 265–298, Feb. 1997.

[25] L. Zeng, D. O'Brien, H. Minh, G. Faulkner, K. Lee, D. Jung, Y. J. Oh, and E. T. Won, "High data rate multiple input multiple output (MIMO) optical wireless communications using white LED lighting," *IEEE J. Sel. Areas Commun.*, vol. 27, no. 9, pp. 1654–1662, Dec. 2009.

[26] L. Yin, W. O. Popoola, X. Wu, and H. Haas, "Performance evaluation of non-orthogonal multiple access in visible light communication," *IEEE Trans. Commun.*, vol. 64, no. 12, pp. 5162–5175, Dec. 2016.

[27] E. S. Sousa and J. A. Silvester, "Optimum transmission ranges in a direct-sequence spread-spectrum multihop packet radio network," *IEEE J. Sel. Areas Commun.*, vol. 8, no. 5, pp. 762–771, June 1990.

[28] I. S. Gradshteyn and I. M. Ryzhik, *Tables of Integrals, Series, and Products*, 7th ed. Academic Press, 2007.

[29] N. L. Bowers Jr., "Expansion of probability density functions as a sum of gamma densities with applications in risk theory," *Trans. Soc. Actuaries*, vol. 18, no. 52, pp. 125–147, 1966.

[30] M. Haenggi, *Stochastic Geometry for Wireless Networks*, 1st ed. New York, NY, USA: Cambridge University Press, 2012.

PLACE PHOTO HERE

Harald Haas (S'98-AM'00-M'03-SM'16-F'17) received the Ph.D. degree from The University of Edinburgh in 2001. He is currently the Chair of Mobile Communications at The University of Edinburgh, and he is the Initiator, Co-Founder, and Chief Scientific Officer of pureLiFi Ltd., and the Director of the LiFi Research and Development Centre, The University of Edinburgh. He has authored 430 conference and journal papers, including a paper in Science and co-authored a book Principles of LED Light Communications Towards Networked Li-Fi (Cambridge University Press, 2015). His main research interests are in optical wireless communications, hybrid optical wireless and RF communications, spatial modulation, and interference coordination in wireless networks. He first introduced and coined spatial modulation and LiFi. LiFi was listed among the 50 best inventions in TIME Magazine in 2011. He was an invited speaker at TED Global 2011, and his talk on Wireless Data from Every Light Bulb has been watched online over 2.4 million times. He gave a second TED Global lecture in 2015 on the use of solar cells as LiFi data detectors and energy harvesters. This has been viewed online over 2 million times. He was elected as a fellow of the Royal Society of Edinburgh and a Fellow of the IEEE in 2017. In 2012 and 2017, he was a recipient of the prestigious Established Career Fellowship from the Engineering and Physical Sciences Research Council (EPSRC) within Information and Communications Technology in the U.K. In 2014, he was selected by EPSRC as one of ten Recognizing Inspirational Scientists and Engineers Leaders in the U.K. He was a corecipient of the EURASIP Best Paper Award for the Journal on Wireless Communications and Networking in 2015 and the Jack Neubauer Memorial Award of the IEEE Vehicular Technology Society. In 2016, he received the Outstanding Achievement Award from the International Solid State Lighting Alliance. He was a co-recipient of recent best paper awards at VTC-Fall, 2013, VTC-Spring 2015, ICC 2016, ICC 2017 and ICC 2018. He is an Editor of the IEEE TRANSACTIONS ON COMMUNICATIONS and the IEEE JOURNAL OF LIGHTWAVE TECHNOLOGIES.

PLACE PHOTO HERE

Liang Yin received the B.Eng. degree (Hons. with Class Medal Award and IET Prize Award) in electronics and electrical engineering from The University of Edinburgh, Edinburgh, U.K., in 2014, where he is currently pursuing the Ph.D. degree in electrical engineering. His research interests are in visible light communication and positioning, multiuser networking, and wireless network performance analysis.